ISSN 2348-6201
Volume 5 Number2
Journal of Advances in Biotechnology

Biogenic synthesis of Iron oxide nanoparticles via optimization of nitrate reductase Enzyme using statistical experimental design

Marwa ELtarahony[1], Sahar Zaki[1], Zeinab Kheiralla[2], Desouky Abd-El-Haleem[1]
[1]Environmental Biotechnology Department, Genetic Engineering and Biotechnology Research Institute (GEBRI), City of Scientific Research and Technological Applications (SRTA-city), 21934 New-Burgelarab City , Alexandria, Egypt,
Tel / Fax: 002034593407.
[2]Botany Department, Faculty of women for Arts, Science and Education, Ain Shams University, Cairo, Egypt

Abstract:

Statistically designed experiments were proceeded to evaluate nutritional and environmental parameters that affect nitrate reductase enzyme (NR) activity in *Achromobacter sp.* **KT735046**. Plackett-Burman design was performed for screening and identifying efficiently the significance of 15 culture conditions influencing NR activity. $FeCl_3 \cdot 6H_2O$, $Na_2MoO_4 \cdot 2H_2O$ and $CuSO_4.5H_2O$ were the most significant variables positively influencing, whereas pH was the most significant negative contributors. The optimal levels of significant factors were further predicted from five level factorial designs, Central Composite Design (CCD). The optimum parameter values were $CuSO_4.5H_2O$ (60.375) mg/l, $FeCl_3 \cdot 6H_2O$ (240 mg /L), pH (6.135) and $Na_2MoO4 \cdot 2H_2O$ (150 mg /L). The biogenic Iron oxide nanoparticles "IONPs" were characterized; the dark brown IONPs exhibit maximum absorption from 400 to 464 nm, XRD reveals crystallite rhombohedral hematite, EDX confirms presence of 62% of iron, TEM illustrates formation of tiny IONPs, 1.4 and 2.8 nm in size, ξ potential and PDI recorded -42.9 mV and 0.268 respectively exhibiting high stability and monodispersed with no agglomeration by the help of biomolecules. This study conclude that *Achromobacter* sp. KT735046 consider being biofactory for synthesis nanoparticles by the help of NR enzyme and it may be the first time to optimize *Achromobacter* sp. KT735046 for IONPs biosynthesis using statistical designs.

Keywords: Nitrate reductase enzyme, Plackett-Burman design, Central composite Design, Iron oxide nanoparticles

Introduction

Iron oxides exist in nature in many forms as supermagnetic magnetite (Fe_3O_4), antiferromagnetic rhombohedral-hexagonal “alpha” hematite (Fe_2O_3), ferrimagnetic cubic"gamma" maghemite, cubic bixbyite structure "beta" paramagnetic and "epsilon" ferromagnetic, orthorhombic structure. Magnetite, hematite and maghemite were the most common forms of Fe (III) [1]. Due to its biocompatibility, it can contribute in biomedical applications such as ferrofluids, magnetic refrigeration, magnetic resonance imaging, biosensors, immunoassays, hyperthermic cancer treatments, drug delivery [2].

Also, IONs can be used as a versatile tool for environmental application due to optical and magnetic properties of it. As in carbon monoxide removal by acting as catalyst and oxidant, elimination of dyes (organic compounds), radioactive metal toxins (*e.g.*, UO2 2+) and adsorption of heavy metals like As, Cr [3,4,5]. By such way, contributing in remediation of different types of contaminants in groundwater, soil and air on both the experimental and field scales.

Synthesis of IONPs can takes place by using various methods as coprecipitation, Sol- gel and forced hydrolysis, hydrothermal, surfactant mediated/template synthesis, microemulsion, electrochemical and laser pyrolysis [6].

These procedures are considered well established, with some advantages such as the production of large quantities of NPs with a controlled size, shape and distribution, in a relatively short time. However, chemical methods are indeed out dated, expensive, complicated, flammable, toxic and produce hazardous wastes, since the use of toxic chemicals (hydrazine, sodium citrate and sodium borohydride) [7] and so limits its application environmentally and biomedically.

Promising alternative procedures were based on the biogenic production of metallic NPs, especially when it overcomes their disadvantages. In this direction, ‘green nanomaterials’ are now a major objective of research in nanotechnology. Green approaches can be performed at ambient temperature and pressure, free of hazardous agents and toxic by-products, clean, less costly and environment-friendly approach. Biogenic IONPs can be synthesized by different organisms, such as, bacteria, plants, algae, yeasts, fungi and actinomycetes. In general, the biogenic synthesis of inorganic metallic NPs led to the formation of NPs capped with proteins/ biomolecules from the organism employed during the synthesis. These capping agents play a key role to prevent nanoparticle aggregation, promoting the stabilization of the nanosystem [6].

Magnetotactic bacteria such as *Geobacter metallireducens* are the most common example on magnetite nanoparticles production under strict anaerobic condition. However, *Actinobacter* spp. is capable of magnetite synthesis by reaction with suitable aqueous iron precursors under fully aerobic conditions [2].

In “biogenic” approach, the nanoparticles are biosynthesized when the microorganisms grab target ions from their environment and then turn the metal ions into the nano / elemental form through enzymes generated by the cell activities. The nitrate reductase was reported in several literatures to be responsible for nanoparticles production especially AgNPs [8, 9]. In all the organisms that synthesize silver nanoparticles nitrate reductase might be an integral part of it.

Nitrate reductases belong to Oxidoreductases that catalyze biological oxidation-reduction reactions. These reactions mediated by microbe control organic oxidations and element cycling in nature, solubilization of metals in the environment which are important concepts in pollution and pollution prevention [10]. Three major types of microbial nitrate reductases can be distinguished, according to the type of nitrate utilization, cellular localization, structure, enzymatic function, biochemical properties and organization /regulation gene. They are the assimilatory cytoplasmic nitráte reductase (NAS), membrane bound respiratory nitrate reductase (NAR), and periplasmic dissimilatory nitrate reductase (NAP). (NAS) occur in eukaryotes as all plants, in most fungi, algae and in many bacteria, is located in the cytoplasmic compartment, is ammonium repressible, participates in nitrogen assimilation by reduction of nitrate to which nitrite is further reduced to ammonia as the final reduction product which is then incorporated into the biomass. In this way, nitrate functions as a source of nitrogen for biosynthetic purposes in the assimilatory pathway. The process may occur under anaerobic conditions and requires energy [11]. (Nar) are involved in anaerobic nitrate respiration and denitrification in which nitrate and nitrite serve as terminal electron acceptors instead of molecular oxygen and are reduced to nitric and nitrous oxides, or further up to gaseous molecular nitrogen. The dissimilatory nitrate reduction is coupled to the generation of the electrochemical proton gradient across the membrane and to generation of ATP. The NAP is unaffected by ammonium or oxygen and are expressed during growth on highly reduced substrates. Different physiological functions have been proposed for the enzyme; however, there are clear evidences that the enzyme is a dissimilatory enzyme used for aerobic denitrification, the transition from aerobiosis to anaerobiosis and the dissipation of an excess reducing power during oxidative metabolism of reduced carbon substrates [11].

It is necessary to achieve the maximum yield of enzyme to meet the industrial requirement in bio-nanotechnology application. No defined media have been established for the optimum production of enzymes from different microbial sources. Each organism has its own special conditions for maximum enzyme production [12]. The main conventional strategy used in media engineering for which the optimal operating condition of a parameter is OVAT. This single dimensional task does not explain interaction effects among the variables on the enzyme production process. Moreover it is a time consuming, laborious practice because of the large number of experiments and often fails to identify the optimal conditions for each factor in this process. To overcome these limitations, statistical approach as RSM was applied

A statistical approach has been employed in the present study for which a Plackett–Burman design is used for identifying significant variables influencing nitrate reductase activity by *Achromobacter Sp.* **KT735046**. The levels of the significant variables were further optimized using Central Composite Design "CCD". The optimized NR producing *Achromobacter Sp.***KT735046** would be applied in biosynthesis of iron oxide nanoparticles "IONPs". The IONPs were then characterized by optical inspection, UV-Vis spectrophotometry, EDX, XRD, TEM, DSL and ξ potential as well.

2. Materials and Methods:

2.1 Chemicals:

All the chemicals were analytical grade and used without further purification obtained from Sigma-Aldrich

2.2 Organism and Culture Maintenance:

The strain *Achromobacter* sp. **KT735046** was isolated from Mariout Lack Basin 3. The pure culture was maintained at $4^{O}C$ and subcultured every 2 weeks. Nutrient broth/ agar "Oxoid" was used in preculture preparation. For long preservation, *Achromobacter* sp. **KT735046** was stored as 1 mL aliquots in 20% glycerol at $-80^{O}C$. The frozen cultures were plated periodically to control their viability.

2.3. Medium and growth conditions:

According to McFarland turbidity standard, cells suspension adjusted to 0.5McFarland (equivalent to about 10^{8} CFU/ml) using sterile saline, was grown on minimal media (Al-Rajhi et al., 2010). The culture was incubated at 30°C at 50 rpm in a rotary shaker for 24 h. After 24 hr. of cultivation, cells were collected by centrifugation at 10000rpm for 15 min, then washed 3 times and re-suspended in 0.1M phosphate buffer. Cells were disrupted by ice cold TSE buffer (20 % sucrose, 5mMEDTA, 0.1M Tris-HCl buffer, pH 8.0) in addition to 10 µl of lysozyme (5 mg/ml); incubation for 30 min at $30^{O}C$ with good vortex every 10 min. The cell debris and unbroken cell will be removed by centrifugation at 10000 rpm for 3 min. The supernatant represent the crude enzyme that will be determined along the optimization experiments [13, 14].

2.4. Assay of nitrate reductase:

The reaction mixture contained (in order of addition): 450 µl of distilled water; 200 µl of 0.5 M phosphate buffer, pH 7.0; 100 µl of 0.2 M KNO3 ; 100 µl of 40 mM benzyle viologen; 50 µl of cell extract; and 100 µl of 0.1 M Na2S2O4 (prepared in 0.3 M NaHCO3). The two blank reactions included, one of them contains inactive enzyme "boiled at $95^{O}C$ for 10 min" and another contains distilled water. After 30 min at $37^{O}C$, the reactions were stopped by vigorous vortex (to oxidize the viologen). 50 µl of 2 M ZnSO4 and 50 µl of 2 M NaOH were added to each mixture, to remove the green debris that could interfere with the spectrophotometric determinations, and the tubes were centrifuged at 10 000 rpm for 1 min. The supernatant was transferred to clean tubes, and then 1 ml of 58 mM sulfanilamide (4-aminobenzenesulfonamide) and 1 ml of 0.77 mM NNEDA (N-(1 naphthyl)ethylenediamine) were added to each mixture to determine the formation of nitrite. After 10 min to allow the appearance of the pink color, absorbance at 540 nm was determined in T60 UV/VIS Spectrophotometer, to calculate nitrite Concentration. One unit of NR activity is the amount of enzyme that catalyzes the formation of 1 µmol of nitrite per minute [13, 15].

2.5. Experimental design and response surface methodology:

2.5.1. Screening for the important factors by Plackett-Burman design "PBD":

The inoculum size % and pH in addition to medium components were evaluated using Plackett-Burman statistical design "PBD". This is a fraction of a two-level factorial design and allows the investigation of '*n*-1' variables with at least '*n*' experiments. According to PBD, the number of (+) is equal to (N+1)/2 and the number of (-) is equal to (N-1)/2 in a row. A column should contain equal number of (+) and (-) signs. All experiments were done in triplicate, and the average NR activity was taken as the response. The main effect was calculated as the difference between the average of measurements made at the high setting (+1) and the average of measurements observed at low setting (−1) of each factor. Table 1 indicates the PB variables and their higher and lower levels. This model describes no interaction among factors and it is used to screen and evaluate the important factors that influence enzyme activity.

TABLE 1: Independent variables and their levels in Plackett-Burman statistical design affecting on NR activity

Variable	Unite	Coded levels / Experimental Values		
		-1	0	1
$MgSO_4.7H2O$	g / L	0.06	0.12	0.18
NaCl	g / L	0.25	0.5	0.75
K_2HPO_4	g / L	0.5	1	1.5
KH_2PO_4	g / L	1.5	3	4.5
NH_4NO_3	g / L	2.5	5	7.5
Yeast-Extract	g / L	2.5	5	7.5
$CuSO_4.5H_2O$	mg / L	20	40	60
$MnCl_2{\cdot}4H_2O$	mg / L	15	30	45
$ZnSO_4{\cdot}7H_2O$	mg / L	155	310	465
$CoCl_2{\cdot}6H_2O$	mg / L	20	40	60
$Na_2MoO4{\cdot}2H_2O$	mg / L	30	60	90
H_3BO_3	mg / L	29	57	86
$FeCl_3{\cdot}6H_2O$	mg / L	120	240	360
pH	_____	6.8	7.5	8.2
Inoculum Size (0.5 McFarland)	%	1	5	10

The factors that have confidence level above 95% are considered the most significant factors that affect the response. The main effect of the medium components, regression coefficient and *P* values of the factors were investigated in the present study. Table 2 shows twenty experimental trials in PBD matrix with selected experimental variables and their NR activity results.

TABLE 2: Plackett-Burman matrix with actual and predicted NR activity

Order no.	dummy Factor	$Na_2MoO4{\cdot}2H_2O$	$FeCl_3{\cdot}6H_2O$	$CoCl_2{\cdot}6H_2O$	Yeast-Extract	NH_4NO_3	KH_2PO_4	H_3BO_3	$CuSO_4{\cdot}5H_2O$	K_2HPO_4	NaCL	$MgSO_4.7H2O$	$ZnSO_4{\cdot}7H_2O$	pH	Inoculum Size %	$MnCl_2{\cdot}4H_2O$	Actual NR activity U/ml	Pred. NR activity U/ml
1	-1	-1	-1	-1	-1	-1	-1	-1	-1	-1	-1	-1	-1	-1	-1	-1	660	635.11
2	-1	1	1	-1	1	1	-1	-1	-1	-1	1	-1	1	-1	1	1	1181.4	1164.

																	3	11
3	1	1	-1	1	1	-1	-1	-1	-1	1	-1	1	-1	1	1	1	160	88.46
4	-1	-1	1	-1	1	-1	1	1	1	1	-1	-1	1	1	-1	1	304.29	232.75
5	-1	1	1	-1	-1	-1	-1	1	-1	1	-1	1	1	1	1	-1	230	301.54
6	1	1	1	-1	-1	1	1	-1	1	1	-1	-1	-1	-1	1	-1	1197.14	1167.82
7	1	-1	-1	1	1	-1	1	1	-1	-1	-1	-1	1	-1	1	-1	587.14	612.03
8	-1	1	1	1	1	-1	-1	1	1	-1	1	1	-1	-1	-1	-1	1120	1090.68
9	-1	1	-1	1	1	1	1	-1	-1	1	1	-1	1	1	-1	-1	137.14	154.46
10	-1	-1	1	1	-1	1	1	-1	-1	-1	-1	1	-1	1	-1	1	68.57	93.46
11	-1	1	-1	1	-1	1	1	1	1	-1	-1	1	1	-1	1	1	880.71	855.82
12	1	-1	1	1	-1	-1	-1	-1	1	-1	1	-1	1	1	1	1	402.14	419.46
13	1	1	-1	-1	-1	-1	1	-1	1	-1	1	1	1	1	-1	-1	164.29	146.97
14	1	-1	-1	-1	-1	1	-1	1	-1	1	1	1	1	-1	-1	1	160.71	131.39
15	1	1	1	1	-1	-1	1	1	-1	1	1	-1	-1	-1	-1	1	516.43	545.75
16	-1	-1	-1	1	-1	1	-1	1	1	1	1	-1	-1	1	1	-1	79.29	61.97
17	-1	-1	-1	-1	1	-1	1	-1	1	1	1	1	-1	-1	1	1	247.14	318.68
18	1	-1	1	-1	1	1	1	1	-1	-1	1	1	-1	1	1	-1	38.57	13.68
19	1	-1	1	1	1	1	-1	-1	1	1	-1	1	1	-1	-1	-1	1015.71	1045.03
20	1	1	-1	-1	1	1	-1	1	1	-1	-1	-1	-1	1	-1	1	428.57	500.11

2.5.2. Central composite design (CCD) method:

pH, $FeCl_3 \cdot 6H_2O$, $Na_2MoO_4 \cdot 2H_2O$ and $CuSO_4.5H_2O$ were four effective variables in the PBD. The variables levels were selected to find the optimum condition for higher NR activity using central composite design (CCD) was shown in Table 3.

TABLE 3: Concentration levels of the independent variables used in central composite design

Variable	Unite	Coded levels / Experimental Values				
		-2	-1	0	1	2
pH	_____	5.8	6.3	6.8	7.3	7.8
$FeCl_3 \cdot 6H_2O$	mg / L	240	300	360	420	480
$Na_2MoO_4 \cdot 2H_2O$	mg / L	30	60	90	120	150
$CuSO_4.5H_2O$	mg / L	30	45	60	75	90

The effect of these variables on enzyme activity was studied at 5 experimental levels: –*a*, –1, 0, +1, + *a*, the concentrations of each level of screened variable are shown in Table 3. CCD includes 8 star points *(a* = 2) and 7 replicates at the center point and16 factorial points. According to this design, the total number of treatment combination is 2^K+2K+n^O were, "k" is the number of independent variables and n^O the number of repetitions of the experiment at the center point. The 31 trail matrix represented in Table 4.

For statistical calculation, the relationship between the coded and actual values is described as the following equation:

$X_i=U_i-U_i^0/\Delta U_i$…… **Equation (1)**

Where X_i is the coded value of the *i*th variable, U_i is the actual value of the *i*th variable, U_i^0 is the actual value of the *i*th variable at the center point and ΔU_i is the step change of variable. The response variable (NR activity) suitable to a quadratic equation for the variables was as following:

$Y = \beta_0 + \beta_1X_1 + \beta_2X_2 + \beta_3X_3 + \beta_{11}X_1^2 + \beta_{22}X_2^2 + \beta_{33}X_3^2 + \beta_{12}X_1X_2 + \beta_{13}X_1X_3 + \beta_{23}X_2X_3$…….. **Equation (2)**

Where: *Y* is the predicted response; Xi, Xj are input variables which influence the response variable Y*;* β_0, intercept; β_1, β_2 and β_3 linear coefficients; β_{11}, β_{22} and β_{33}, squared or quadratic coefficients β_{12}, β_{13}, and β_{23}interaction coefficients.

TABLE 4: Experimental & predicted values of NR activity of Five – Level Central composite Design "CCD" of four variables

Run Order	pH	$CuSO_4.5H_2O$	$Na_2MoO4{\cdot}2H_2O$	$FeCl_3{\cdot}6H_2O$	"Experimental" NR Activity U/ml	"Predicted" NR Activity U/ml
1	1	-1	-1	1	2111	2127.917
2	2	0	0	0	1605	1652.458
3	1	1	1	1	1690	1649.083
4	0	0	0	0	2168	2167.143
5	0	0	0	2	2003	2000.292
6	1	1	1	-1	2009	1949.958
7	0	2	0	0	1200	1373.292
8	1	-1	-1	-1	1610	1635.792
9	0	0	0	0	2169	2167.143
10	0	-2	0	0	1600	1479.792
11	1	1	-1	1	2087	2015.792
12	-1	1	1	1	1580	1502.292
13	1	1	-1	-1	1950	1900.417
14	-1	-1	-1	-1	1511	1550.75
15	0	0	-2	0	2440	2470.625
16	0	0	0	0	2178	2167.143
17	1	-1	1	1	2105	2155.458
18	-1	1	-1	1	1800	1819.25
19	-2	0	0	0	1415	1420.625
20	-1	1	-1	-1	2053	1950.625
21	0	0	0	-2	2000	2055.792
22	0	0	0	0	2187	2167.143
23	-1	-1	-1	1	1789	1796.125

24	0	0	2	0	2575	2597.458
25	-1	-1	1	1	1825	1873.417
26	0	0	0	0	2188	2167.143
27	1	-1	1	-1	2100	2079.583
28	-1	1	1	-1	2068	2049.917
29	-1	-1	1	-1	2025	2044.292
30	0	0	0	0	2100	2167.143
31	0	0	0	0	2180	2167.143

2.5.3. Statistical analysis:

Minitab 14.0 (Minitab Inc., Pennsylvania, USA) was used for establishing the experiments designs "matices" and subsequent regressional analysis of the experimental data of both "PDB and CCD". And statistical analysis of the model was performed to evaluate the analysis of variance (ANOVA). The quality of the polynomial model equation was judged statistically by the coefficient of determination R^2, and its statistical significance was determined by an F-test. In addition to 3D surface plots, contour plots and application for optimizer.

2.5.4. Validation of Experimental model:

The statistical model was validated for NR activity under conditions predicted by model and compared with anti-optimized and original media.

2.6. Biosynthesis of IONPs:

3 mM of Fe $(NO_3)_3.9H_2O$ was added to the optimized media was used for growing *Achromobacter* sp. **KT735046** under 50 rpm and 30^{O}C in order to produce IONPs. After incubation period, the cells containing IONPs were collected by centrifugation at 10000rpm for 20 min and disrupted as described previously. The IONPs were characterized as follows:

2.7. Characterization for IONPs:

2.7.1. Optical Observation:

The reduction of Fe $(NO_3)_3.9H_2O$ ions to IONps could be optically examined by color changes of the bacterial cells and slightly surrounding media.

2.7.2. UV-Vis spectroscopic analysis:

The biosynthesized IONps were preliminary characterized by UV-Vis spectrophotometer (Labomed. model UV–Vis Double beam spectrophotometer) in the wavelengths ranging from 200-800 nm by using of double inoculation media containing 3 mM of $Fe(NO_3)_3.9H_2O$ as blank.

2.7.3. XRD Analysis of Synthesized Iron Oxide Nanoparticles:

The crystalline nature, quality and crystallographic identity of the examined material in addition to the phase purity were determined by X-ray Diffraction. The IONPs were coated microscopic slide and let it to dry in an oven at 37 ºC for 48 hour then was analyzed by X-ray Diffractometer (Schimadzu-7000, USA). XRD spectrum with Cu Kα radiation λ=1.504A° over a wide range of Bragg angles 10°≤ 2θ ≤ 80. X-ray tube operated at 30 kV/ 30 mA. The scan speed was 4^{0}/min.

2.7.4. Dispersive X-ray Spectra (EDX):

The chemical composition of the biosynthesized IONp was examined using EDAX using (JEOL JSM 6360LA, Japan - Faculty of Science- Alexandria University) scanning electron microscope equipped with EDS controlled system.

2.7.5. Dynamic light scattering and ξ potential:

The electrostatic potential, particle size measurement "hydrodynamic diameter" and particle size distribution of IONps were performed through DLS technique using Zetasizer Nano ZS (Malvern Instruments, Worcestershire, UK; Faculty of pharmacy-Alexandria University). The IONps was equilibrated at 25°C for 120 sec in a zeta cell then placed in the analyzer chamber equipped with a HeNe laser operating at 632.8 nm and a scattering detector at 173 degree. The data were analyzed by Zetasizer software 6. The results were expressed as the mean ± standard deviation (SD) of at least two independent measurements (Zetasizer Nano Series User Manual, 2004).

2.7.6. Transmission electron microscope (TEM):

TEM has been employed to characterize the size, shape, and morphologies of the formed IONPs and its producing cells using Transmission electron microscope TEM (JEOL JEM-1230, Japan- Faculty of Science- Alexandria University).

3. Result and Discussion:

3.1. Screening of parameters using Plackett–Burman design

Two level of each component in the design was examined along with 20 experimental run conducted in duplicate indicating variation of NR activity from 38 U/ml to 1197 U/ml as indicated in Tables 2. The regression coefficients of the model were analyzed statistically by MINITAB 14 indicates that pH (confidence level =99.9 %, P-value 0.0014), $FeCl_3 \cdot 6H_2O$ (confidence level =98.7 %, 0.013 P-value), $Na_2MoO_4 \cdot 2H_2O$ (confidence level =98.6 %, 0.014 P-value) and $CuSO_4.5H_2O$ with confidence level =97.8 %, 0.022 P-value) consider as the significant parameters. As larger the magnitude of the *t*-value and smaller the *p*–value (prob > F <0.05) the greater is the significance and effect of the corresponding coefficient term on the response. From normal probability plot of effects Figure 1, it is clear that $FeCl_3 \cdot 6H_2O$, $Na_2MoO_4 \cdot 2H_2O$ and $CuSO_4.5H_2O$ have a positive effect on the model response (increasing in NR activity in higher concentration) Since they lie on right hand side of the line, while pH influence negatively on its activity (i.e. increasing in NR activity accompanying with low pH) as seen as lie on left hand side of the line. As they lied furthest from the line, the largest effect was exhibited. The rest of the effects lies along the line are negligible.

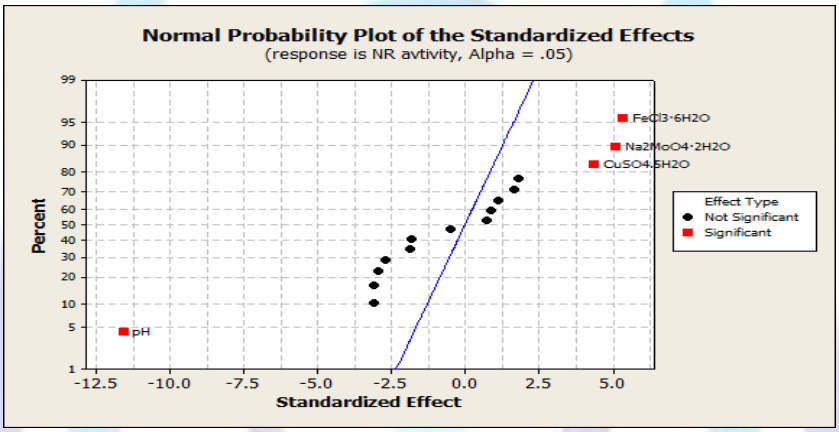

FIGURE 1: Normal probability plot of variables effects on NR activity

As reported in literatures, NR enzymes belong to the DMSO reductase family. As a rule, all studied NRs share a common property, the presence of Mo^{6+} Molybdenum cofactor (Mo-co) and Fe^{3+} [4Fe-4S] is required for the cytochrome subunits, at which is incorporated into the enzyme active center in catalytic subunit [15, 16]. The significant effect of copper can be suggested to its using in the multi-copper oxidase CueO that is thought to acquire copper in the cytoplasm, and the cytoplasmic pathway for molybdopterin cofactor synthesis that is bound to the nitrate reductase [17, 18]

On contrary to this study, another point of view postulated that, an inorganic combination of molybdenum and copper or sulphur, or $MO^{+} Cu^{+} S$, a result in the formation of an insoluble copper thiomolybdate complex salt which inhibit nitrate reductase. That case was reported in rumen micro-organisms [19]. This finding clearly indicates that the effect of metal ions on reductase activity depends on the type of microbial cell used as biocatalyst in bioconversion reactions [20].

For Hydrogen Ion Concentrations "pH", is influenced negatively on *Achromobacter sp.* **KT735046**. At such acidic conditions, the bonds within NR molecules are influenced by H^+ and OH^- ions in such a way that the shape of their active site is the most complementary to the shape of their substrate "NO3". Also alternation in pH can cause changing in protonation state of the substrate and subsequently its binding to enzyme [21], and by this way, the rate of reaction is at an optimum level.

From the standard analysis of variance (ANOVA) summary calculated from experimental runs, the model appears to be significant. As P-value that is the probability that magnitude of a contrast coefficient is due to random process variability is small ~ 0.021 (P< 0.05) in addition, R^2 was 0.9885 and adjusted R^2 0.9275 % which examines the overall performance of the model. When R^2 is closer to the 1, the better the estimation of regression equation fits the sample data. Also implying that 98.85% of the variability of the data can be explained by the model. While there was only a 1.15% chance that could occur due to noise. This again ensured a satisfactory adjustment. On application of ANOVA, it was found that the first order model for NR activity was fitted to the results obtained from the 20 experiments as the Following equation:

Y (NR activity) =479 – 11.9 dummy factor + 122.6 $Na_2MoO_4 \cdot 2H_2O$ + 128.5 $FeCl_3 \cdot 6H_2O$ + 17.7 $CoCl2 \cdot 6H_2O$ +43 Yeast Extract +39.8 NH_4NO_3– 64.8 KH_2PO_4 -44.4 H_3BO_3 + 105 $CuSO_4.5H_2O$ – 74.2 K_2HPO_4 – 74.2 NaCL- 70.4 $MgSO_4.7H_2$ + 27.4 $ZnSO_4 \cdot 7H_2O$ – 277.7 pH + 21.4 inoculum size %- 44 $MnCl_2 \cdot 4H_2O$…… **Eq. (3)**

3.2. Response surface methodology:

The CCD design was employed to study the interactions among the significant factors and also determine their optimal levels. The other variables in the study were maintained at a constant level which gave maximal yield in the PB experiments. The results are represented in Table 4. Multiple regression analysis was used to analyze the data and thus a second-order polynomial equation was derived from regression analysis as follows:

Y (NR activity) = 2167.14+ 57.96 pH- 26.62 $CuSO_4.5H_2O$+31.71 $Na_2MoO_4{\cdot}2H_2O$- 13.87 $FeCl_3{\cdot}6H_2O$- 157.65 $(pH)^2$-185.15 $(CuSO_4.5H_2O)^2$+ 91.72$(Na_2MoO_4{\cdot}2H_2O)^2$ - 34.78$(FeCl_3{\cdot}6H_2O)^2$ - 33.81pH*$CuSO_4.5H_2O$ -12.44pH* $Na_2MoO_4{\cdot}2H_2O$ + 61.69pH* $FeCl_3{\cdot}6H_2O$ - 98.56 $CuSO_4.5H_2O$ *$Na_2MoO_4{\cdot}2H_2O$ - 94.19 $CuSO_4.5H_2O$* $FeCl_3{\cdot}6H_2O$ - 104.06 $FeCl_3{\cdot}6H_2O$* $Na_2MoO_4{\cdot}2H_2O$……**Equation (4)**

The adequacy of the model was checked using analysis of variance (ANOVA) which was tested using Fisher's statistical analysis and the results are showed in Table 5. The model P value of 0.00 implies the model is significant. Lack of fit test was also performed. It describes the variation in the data around the fitted model that was testified. The insignificant lack of fit indicates a good model. Although lack of fit of this model was significant (p values 0.006) but its F-value was small when compared to F-value of model. Due to that, the model was considered to be good and fitted well to the experimental data.

TABLE 5: Estimated regression coefficients for second order polynomial model of NR activity

Term	Coef.	SE Coef.	T	P
Constant	2167.14	29.14	74.364	0.000
pH	57.96	15.74	3.683	0.002
$CuSO_4.5H_2O$	-26.62	15.74	-1.692	0.110
$Na_2MoO_4{\cdot}2H_2O$	31.71	15.74	2.015	0.061
$FeCl_3{\cdot}6H_2O$	-13.87	15.74	-0.882	0.391
$(pH)^2$	-157.65	14.42	-10.934	0.000
$(CuSO_4.5H_2O)^2$	-185.15	14.42	-12.841	0.000
$(Na_2MoO_4{\cdot}2H_2O)^2$	91.72	14.42	6.362	0.000
$(FeCl_3{\cdot}6H2O)^2$	-34.78	14.42	-2.412	0.028
pH * $CuSO_4.5H_2O$	-33.81	19.28	-1.754	0.099
pH * $Na_2MoO_4{\cdot}2H_2O$	-12.44	19.28	-0.645	0.528
pH * $FeCl_3{\cdot}6H_2O$	61.69	19.28	3.2	0.006
$CuSO_4.5H_2O$ * $Na_2MoO_4{\cdot}2H_2O$	-98.56	19.28	-5.113	0.000
$CuSO_4.5H2O$ * $FeCl_3{\cdot}6H_2O$	-94.19	19.28	-4.886	0.000
$Na_2MoO_4{\cdot}2H_2O$ * FeCl3·6H2O	-104.06	19.28	-5.399	0.000
R-Sq = 96.6%		**R-Sq(adj) = 93.5 %**		

The goodness of fit of the model and compatibility of experimental data with predicted were checked by the determination coefficient (R^2), which was calculated to be 0.966, implying that 96.6% of the variability in response could be explained by the model, whereas only 3.4 % of the total variations was not explained by the model. The R^2 value was always between 0 and 1, and a value > 0.75 indicated the aptness of the model [22]. The adjusted R^2 value corrects the R^2 value for the sample size and for the number of terms in the model. The value of the adjusted determination coefficient (Adj R^2 = 0.935) was also high, advocating the high significance and adequacy of the model. The model coefficient of variation (CV) is 15.6. So model can be considered to be somewhat reproducible in addition to reliability of the experiments performed. (CV) indicates the degree of precision with which the experiments are compared. The lower reliability of the experiment is usually indicated by high value of CV. Another item in model validation was Normal probability plot, which was graphical method that can be used to characterize the nature of residuals of the models. It is clear from Figure 2 that the residuals followed normal distribution as well as majority of the data points are distributed along the line normal (followed the fitted line as in high degree of vicinity of the points to the straight-line) with very few outliers indicating little skewed. The residual plot doesn't shows any trend in addition exhibiting equal scatter of the residual against fitted value of the model indicates that the variance was independent of the NR activity, thus supporting the adequacy of the model fit.

ISSN 2348-6201
Volume 5 Number2
Journal of Advances in Biotechnology

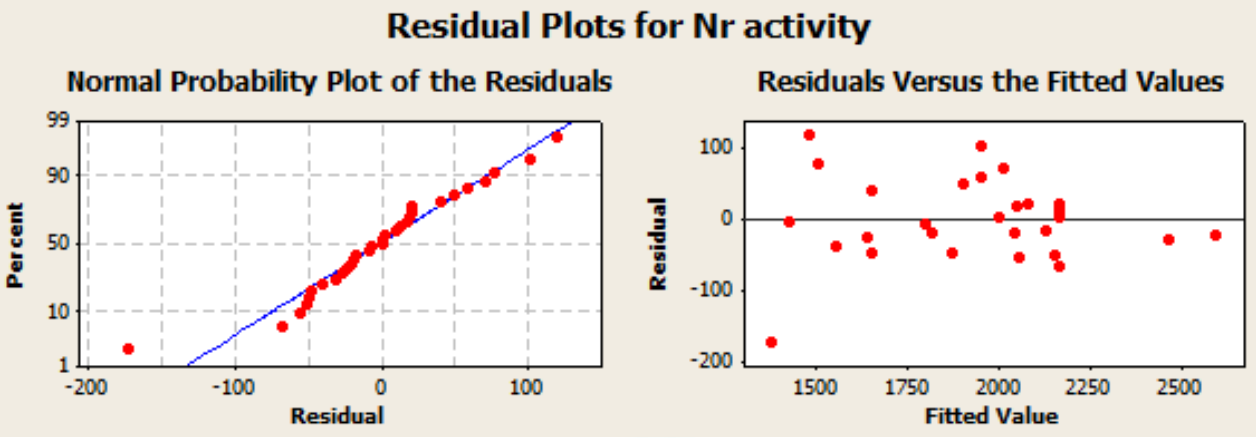

FIGURE 2: A-Normal probability plot of residuals against NR activity percentage &B- Residual distribution against fitted values plot of CCD

Studentized residual is the residual divided by an estimate of its standard deviation. The residuals were studentized and values which were greater than +2 and less than −2 were considered as large [23]. Obtaining a smaller residual value is preferred as this shows the degree of deviancy from predicted model. As obtained in both PB & CCD the residuals values fall in this acceptable range.

The empirical functional relationship between the response and significant factors represented by the 3D response surface plot and 2D contour plots. At which the response (NR activity) expressed at the vertical axis and two explanatory factors on horizontal axes in their coded levels of, while the remaining factors being held at constant levels.

The effect of pH and $CuSO_4.5H_2O$ interaction on NR activity is represented graphically at Figure 3. The surface plot was convex suggest that there are well-defined optimal variables. ; Plus, as the variable ranges were appropriate; the optimum lies in the design space. As noticed the NR activity increase with increasing pH while decreasing $CuSO_4.5H_2O$ concentration and vice versa. Further increase in variables values leads to decrease in NR activity. The stationary point appeared at the maximum of curvature which revealed its presence within the central range. With respect to its prospective contour plot, it reveals that interaction between pH and $CuSO_4.5H_2O$ was neglicable as the contour plot was circular.

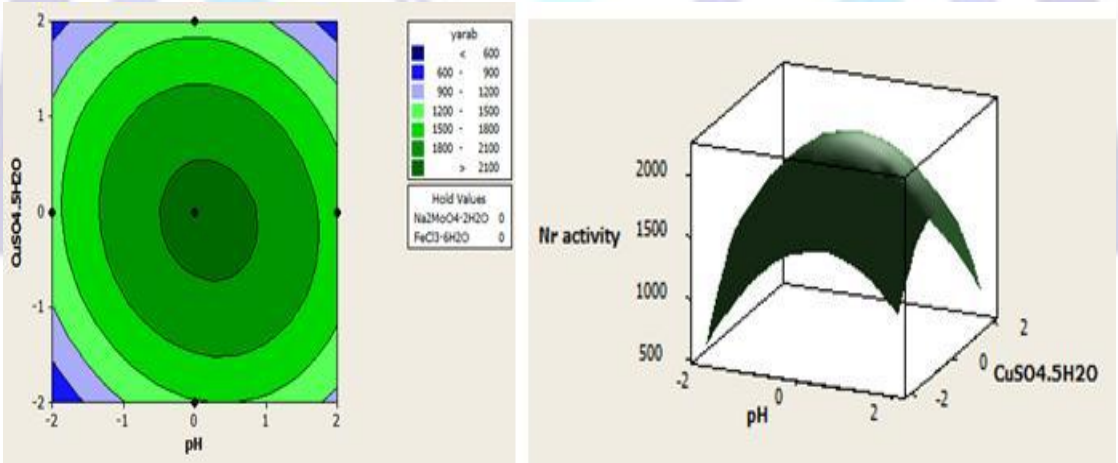

FIGURE 3: a- Surface plot b- Contour plot for NR activity Showing the interactive effects of pH and $CuSO_4.5H_2O$ with other variables at central points

Surface plot and contour plot of mutual interaction effect of $FeCl_3 \cdot 6H_2O$ and pH on NR activity indicated in Figure 4.While, keeping the other variables at its center levels. NR activity increase with increasing in both variables simultaneously until reaches to the maximum level then began to decline with more increasing in variable values. That is may be due to negative quadratic effect. The surface plot of this interaction exhibits broad hump and flat near the optimum indicating that the optimized values may not vary widely from the single variable conditions. This notice confirmed through the contour plot, at which, elliptical shape indicating significant synergetic interaction.

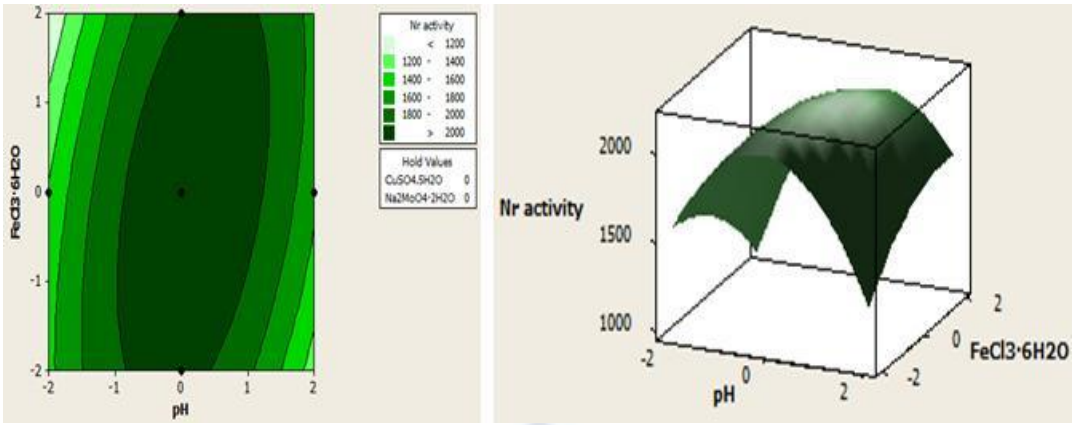

FIGURE 4: a- Surface plot b- Contour plot for NR activity from showing the interactive effects of pH and $FeCl_3 \cdot 6H_2O$ with other variables at central points

An antagonistic effect $Na_2MoO4 \cdot 2H_2O$ and $FeCl_3 \cdot 6H_2O$ on NR activity was graphically illustrated in Figure 5 indicating ridged surface plot and the stationary

point was a saddle point for the response. From its corresponding contour plot, the maximum NR activity > 2800 U/ml can be achieved at the 150mg of

$Na_2MoO4 \cdot 2H_2O$ concentration with the lowest $FeCl_3 \cdot 6H_2O$ concentration (240 mg) or at 30 mg $Na_2MoO4 \cdot 2H_2O$ and 480 mg of $FeCl_3 \cdot 6H_2O$ which located at the upper

left and down right corner with darker shadow. Elliptical saddle contour plot also reveal presence of significant interaction effect of two independent variables on NR

activity.

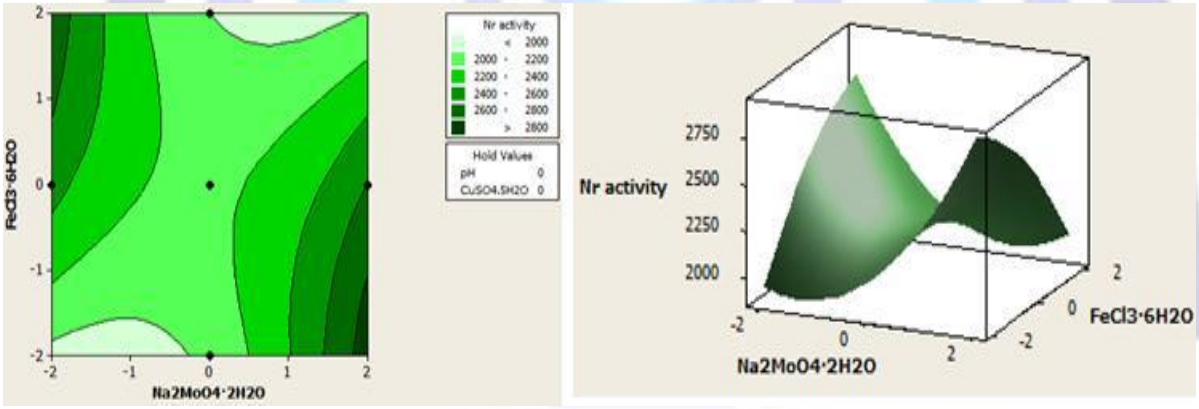

FIGURE 5: a- Surface plot b- Contour plot for NR activity from showing the interactive effects of $Na_2MoO4 \cdot 2H_2O$ and $FeCl_3 \cdot 6H_2O$ with other variables at central points

The reduced regression model was solved for maximum NR activity using the response optimizer tool in MINITAB 14.0. Minitab's Response Optimizer calculates individual desirability using a desirability function (also called utility transfer function). An optimal solution occurs where composite desirability obtains its maximum. Desirability has a range of zero to one. One represents the ideal case; zero indicates that one or more responses are outside their acceptable limits.

Response optimizer was used to identify the exact optimum combination of the test variable that jointly optimizes a response "NR activity" which leads to achieving response goals. The results of the response optimizer at optimum condition for maximum goals are shown in Figure 6.

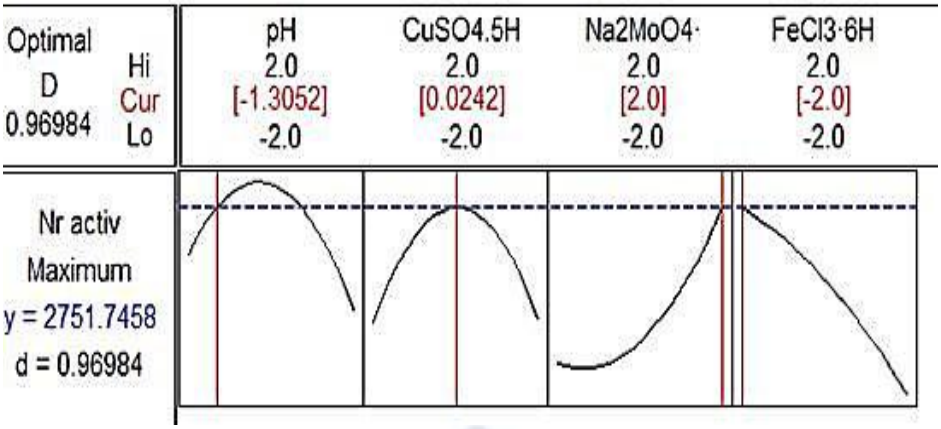

FIGURE 6: Response optimizer at with desirability function, for NR activity with maximum goal

The value of *"d"* increases as the "desirability" of the corresponding response increases. The factor settings with maximum desirability are considered to be the optimal parameter conditions. it was observed that desirability value recorded 0.969 which was closed to indicating the setting seem to achieve favorable results for maximizing NR activity value The optimum parameter values were as follows: $CuSO_4.5H_2O$ = 60.375 mg/l, $FeCl_3 \cdot 6H_2O$ =240 mg /L, pH = 6.135 and $Na_2MoO4 \cdot 2H_2O$ =150 mg /L .all of which were located within the experimental range to predict NR activity to be 2751.7 U/ml.

3.3 Experimental verification of the model:

In order to validate these results, experiments were done in triplicate at the optimized values as suggested by RSM. Under the optimized conditions, the predicted response for NR activity was 2751.7 U/mL and the average of observed experimental values was 2687.9 U/ml. Difference between the predicted and the experimental is 2.2 % which considers being small. This optimization strategy led to the enhancement of NR activity from 1119 U/mL (basal medium) to 2592.6 U/mL (optimized medium) with 2.4-fold increase. Whereas, anti -optimum conditions resulted in 300 U/ml with 8.6 fold decrease from optimized conditions. In this study, statistical methods approved to be valuable tool for the rapid screening, optimization of multiple variables simultaneously and predict the best performance conditions with minimum number of experiments, also reflect the role of each of the components, their interactions in elevating enzyme activity [24].

Nicholas *et al*., [25], reported that 10 µg/l of Molybdenum and 1.5 mg/l of Fe^{+3} were required for maximum nitrate reductase activity of *Photobacterium sepia* (*Achrornobacter Jischeri).* Whereas, *Kim et al.,* [26] used basal media containing about 0.012 gm/l of Na_2MoO_4 and 0.05gm/l $FeSO_4$ to cultivate the denitrifying bacteria *Ochrobactrum anthropic* SY509 which exhibited excellent activity on dissimilative nitrate reduction in anaerobic condition. In addition, the most adequate pH for nitrate reduction always in the neutral to slightly alkaline conditions (6.5-7.8) with different bacterial species as of *Thiosphaera*, *Paracoccus, Achromobacter, Alcaligenes, Bacillus, Flavobacterium, Corynebacterium* [27, 28, 29].

3.5. Correlation between NR activity and cell density:

Along with all optimization trails both NR activity and cell density (data not shown) were

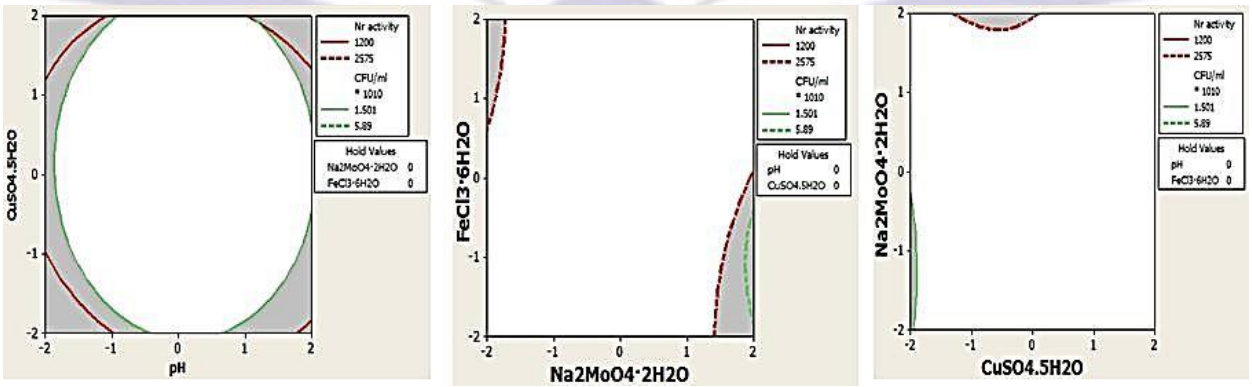

FIGURE 7: Overlaid contour plot of NR activity and biomass

determined simultaneously. In order to verify correlation between both NR activity and cell density graphically, the overlaid contour plot was used. The overlaid plot investigated the combination of parameters levels that satisfied the requirements placed on each of the responses; the bright area in Figure 7 shows the feasible response values in the factor space. Such bright region was delimited by 2 colored lines the red one represent NR activity in high and low values and green line that represent cell density in high and low values. Regions that did not meet the proposed criteria were shaded. The white areas on the plots signify the restrictions that must be placed on the system to achieve the desired result.

The overlaid contour plots summarize the matching and oneness between both responses and the levels of examined variables. This confirms that exact parameters with approximately exact levels of them were required to achieve maximum values for both NR activity & cell density. This point of view opposes [30, 31] that suggested NR activity present in cell free supernatant of *B. subtilis* and *Bacillus stearothermophilus*

3.5. IONPs characterization:

3.5.1 Optical Observation:

The reduction of $Fe(NO_3)_3.9H_2O$ ions to IONps could be optically approved by color changes of the bacterial cells and slightly surrounding media from yellow to dark brown / black as illustrated in Figure 8. However, such color changes occurred might be due to the variation in the nature, size and shape of the metal particles by relative activity of bacterial cell.

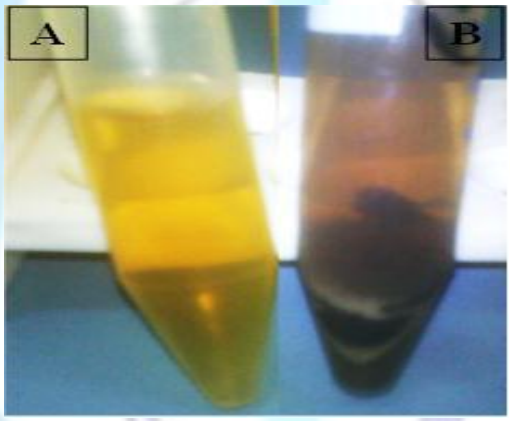

FIGURE 8: Visual inspection of IONPs synthesized by cell A: Media containing 3mM $Fe(NO_3)_3.9H_2O$ "before inoculation" B- Biosynthesized IONPs in cells and in surrounding media.

3.5.2 UV-Vis spectroscopic analysis:

UV-Vis absorption spectra of biosynthesized IONps was shown in Figure 9 exhibiting the maximum range from 400 to 464 nm reflecting the nanoparticles surface plasmon resonances (SPRs). Such result in agreement with [32, 33, 34]. While, Batin and Popescu [35] reported that absorbance peak of hematite nanoparticles was in range of 560-572. Balamurughan *et al.,* [36] reveals that UV visible spectra showed the maximum absorbance at 285 and 324 nm.

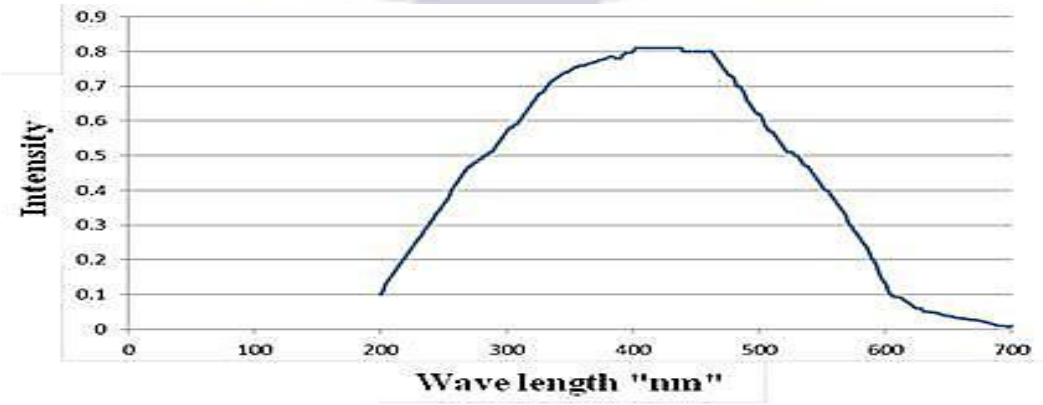

FIGURE 9: UV-Vis absorption spectrum IONPs synthesized by cells

3.5.3. XRD Analysis of Synthesized Iron Oxide Nanoparticles:

XRD pattern is characterized by the interplanar d- spacing / 2θ degree and the relative intensities (I/I0) of the strongest peaks. It was found out the 2θ degree position of the examined sample related to haematite as illustrated in Figure 10.

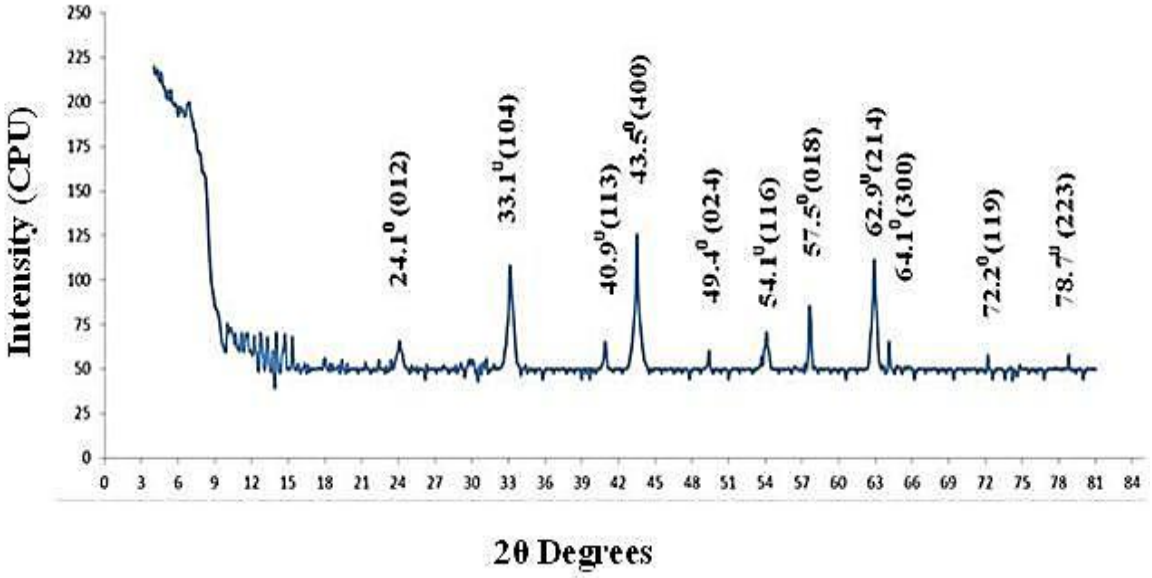

FIGURE 10: XRD crystallography of biosynthesized IONPs

The diffraction peaks of IONPs positioned at 24.1^0, 33.1^0, 40.9^0,43.5^0 49.4^0, 54.1^0, 57.5^0, 62.9^0, 64.1^0, 72.2^0 and 78.7^0 that were corresponding to Miller indices of 012, 104, 113, 400, 024, 116, 018, 214, 300, 119 and 223 planes respectively. The XRD peaks of haematite were clearly distinguishable, sharp and broad, that reveals the ultra-fine nature, purity and crystallite sizes of the biosynthesized IONPs. XRD pattern was indexed to rhombohedral in their position according to (JCPDS card no. 33-0664) which in agreement with [32, 37, 38].

3.5.4. EDX:

The EDX analysis detailed the elemental composition of the nanoparticles, confirming the presence of iron as illustrated in Figure 11.The atomic percentage of the sample elements reveals strong signal in the iron region with 62.1 % which confirms the formation of iron nanoparticles. Absence of oxygen from EDX spectral analysis is attributed to old version of EDX instrument that was unable to detect it.

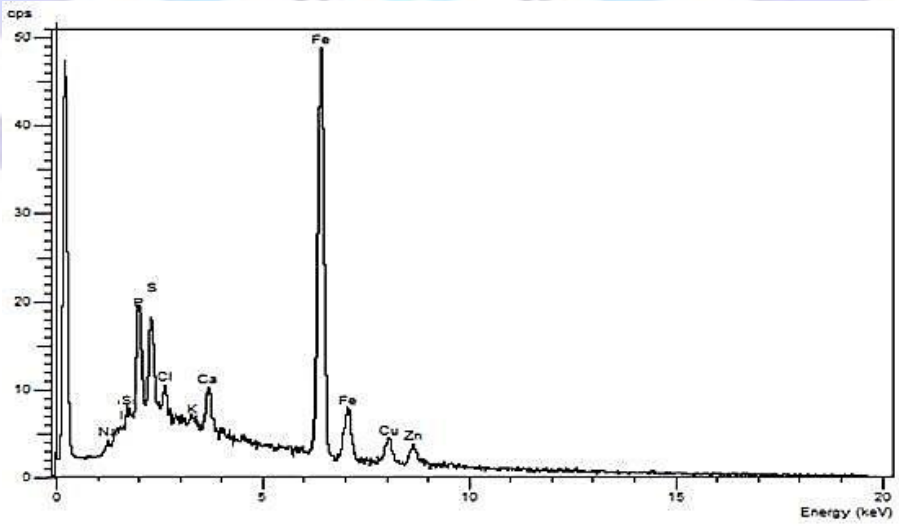

FIGURE 11: EDX pattern of IONps sample

The other peak for S and P present also in large percent indicated by 10.2 and 11.4 % respectively. Such point could be explained by the presence of bacterial biomolecules that contain polar phosphorus backbone as phospholipids [39], ATP [40], DNA [41] and RNA [42]. With respect to sulfur, it considers being an important structural and functional component of proteinogenic amino acids as cysteine, methionine. Other elements were detected in EDX spectrum but in small percentage as Ca, Zn and Cu that also represents an essential ingredient in bacterial structural proteins that have functional groups [43].

3.5.5. Dynamic Light Scattering "DLS" and Zeta "ξ" potential analysis:

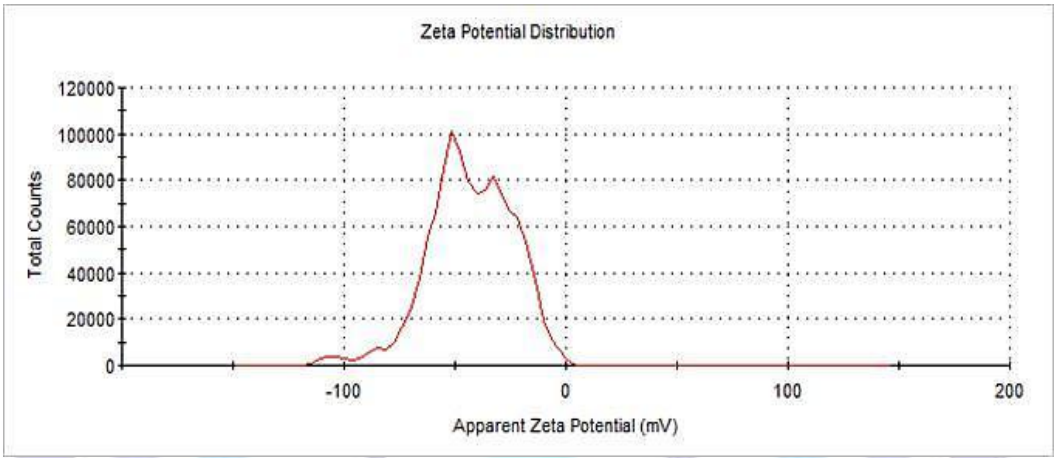

FIGURE 12: ξ potential of biosynthesized IONPs

The electrostatic potential (The Zeta potential "ξ") that exists at the shear plane of a particle, which is related to both surface charge and the local environment of the particle was -42.9 mV with 202, 36 and 6.5nm as 25.8%, 45.2% and 29% in intensity as "hydrodynamic diameter". All results as a mean of 3 measurements were indicated in Figure 12. ξ potential of the nanoparticles give an idea about the stability in the medium it is dispersed in. As described in literatures, both theoretical and practical, zeta potential can lie anywhere in the range of –100 to +100 mV [44]. However, a dividing line between stable and unstable aqueous dispersions is generally taken at either +30 or -30mV and in other literatures +25 mV / -25 mV, which means that particles with zeta potentials more positive than +30mV are normally considered stable, as well as the particles with zeta potentials more negative than -30mV [45].

ξ potential of biosynthesized IONPs was found to be advantageous as recorded a higher value which is due to greater electro-static repulsion between the particles that results in "Brownian motion". Such motion keep them in a state of animated suspension for a much longer time and by such way minimizing aggregation/flocculation and exhibiting monodispersion and colloidal stability [46, 47, 48].

The negative singe of ξ potential is due to bacterial proteins which IONps was suspended in. Such bacterial proteins which carrying negative charge suggested being due to negatively charged amino acid as aspartate and glutamate [49]. According to Nilsson and Heijne [50] the negatively charged amino acid residues were acidic due to the carboxyl groups side chains [51]. In addition to presence of polar negatively charged phosphate group (PO_3^-) along the sugar-phosophate backbone within nucleic acid residues including both DNA and RNA [52]. The result of ξ potential supports the result of RSM, where *Achromobacter sp.* **KT735046** favors acidic conditions (pH 6.135) to maximum enhancement of metabolic activity, which suggested being general character and behavior of such strain.

IONs appeared to be stabilized by such amino acid residues, DNA and RNA consider acting as capping, stabilizing and functionalizing agent which preventing aggregation and agglomeration. That conclusion in agreement with several reports where using naturally occurring biopolymers as reducing and stabilizing agents for various nanoparticles types [53, 54] which reporting that binding of proteins to nanoparticles either through free amino groups or by electrostatic interaction of negatively charged carboxylate groups. By such way proteins and polysaccharide considered as stabilization and functionalization agents for Nps.

The particle size distribution is reported as a polydispersity index (PDI) was 0.268 which implies that biosynthesized IONPs was homogenous dispersity. At which, the range for the PDI is from 0 to 1, values close to zero indicate a homogeneous dispersion, and those greater than 0.5 indicate high heterogeneity [55]. There is a direct correlation existing between zeta potential, PDI, and particle size. The salient conclusion is that larger the negative zeta potential lower will be the particle size and PDI cause the particles remaining discrete without agglomeration. And that was harmonious with [37, 56, 57].

On comparing ξ- potential of free cell supernatant inoculation (data not shown), it was observed that, zeta potential was -13.4 mV and particle size 900 nm and 36 nm with 93% and 7% intensity respectively. On the other hand, the zeta potential and particle size of cultivation media containing [3 mM of $(FeNO_3)_3.9H_2O$] were as follows: 4.6mV, 5.382µm (3%

intensity), 321nm(97% intensity). The negative sign zeta potential of cell free supernatant was due to external metabolites, extracellulare proteins and lipopolysaccharide which excreted from the cell into surrounding media. Whereas, media containing IONp precursor was positive due to media components emphasizing effect of bacterial cells and its biomolecules on IONps production, stabilization and monodispirsity. The results from both cases lying in instability range and large particle implies tendency for aggregation [46].

3.5.6. Transmission electron microscope (TEM):

TEM has been employed to characterize the size, shape, and morphologies of the formed IONPs and its bio factory. During TEM analysis, Particles with higher electron density will appear darker in the TEM negative film.

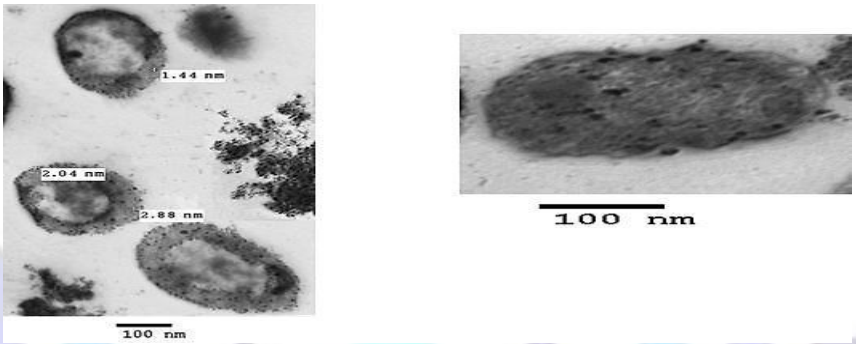

FIGURE 13: TEM micrograph of IONPs and its producing cells

As illustrated from Figure 13, bacteria seem being at exponential phase containing teeny, uniform, spherical, monodispersed without distinct aggregation electron opaque nanoparticles. It ranging in size from 1.4 to 2.8 nm and scattered as seeds like in the periplasmic space of the bacterial cells. That could be attributed to the localization of NR enzyme that was periplasmic and cytoplasmic membrane. During the catalysis, nitrate is converted to nitrite, and an electron will be shuttled to the incoming metal ions that were reduced and deposited in periplasmic space and some of it release outside the cell as described by [58]. Such results were resembled synthesized AgNPs within its periplasmic space of *Pseudomonas stutzeri* AG259 and *B. licheniformis* [58, 59].

Nanoparticle synthesis microbially consider being way for detoxification of metals , where, microbial systems can detoxify the metal ions by extracellular precipitation of soluble toxic inorganic ions to insoluble non-toxic metal nanoclusters, reduction and. intracellular bioaccumulation as noticed in this study [60].

Achnowledgment

This work was supported by PhD grant from the Egyptian *Academy* of *Scientific Research* and *Technology* (C-15).

5. References:

[1] Rajendran K. and Shampa S. 2013. Biogenic Magnetite Nanoparticles, *Research Journal of Pharmaceutical, Biological and Chemical Sciences,* vol. 4, no. 3, pp. 1037-1043.

[2] Atul B., Aijaz W., Yogesh S., Pattayil A. J., Bhagavatula L. V. and Murali S. 2005. Bacterial Aerobic Synthesis of Nanocrystalline Magnetite. *Journal American Chemistry Society* vol. 127, pp. 9326-9327.

[3] Faraji M., Yamini Y.and Rezaee M. 2010.Magnetic Nanoparticles: Synthesis, Stabilization, Functionalization, Characterization, and Applicati ons", *Journal Iranian Chemistry Society*, vol. 7, no. 1, pp. 1-37 .

[4] Samuel C.N. and Irene M.C. 2 0 1 3. Magnetic nanoparticles: Essential factors for sustainable environmental applications. *Water Research, vol.* 4, no. 7.

[5] Joya, J. B., Jaimez . M. R. and Ortega J. B.. 2013. Preparation and characterization of Fe_2O_3 nanoparticles *Journal of Physics: Conference Series,* vol. 466.

[6] Amedea B. S., Paula H., Nelson D. 2013. Biogenic synthesis of nanostructured iron compounds: applications and perspectives. *IET Nanobiotechnology,* vol. 7, no. 3, pp. 90–99.

[7] Gholampoor N., Emtiazi G.and Emami Z, 2015. The Influence of *Microbacterium hominis* and *Bacillus licheniformis* Extracellular Polymers on Silver and Iron Oxide Nanoparticles Production; Green Biosynthesis and Mechanism of Bacterial Nano Production. *Molecular Nanotechnology,* vol. 4, no. 2.

[8] Silambarasan S. and Abraham J. 2013. Biosynthesis of silver nanoparticles. *African Journal of Biotechnology*. vol. 12, no. 21, pp. 3088-3098.

[9] Zaki S., Kamal A., Elkady M., Abu-Elreesh G. and Abd-El-Haleem D. 2014. Biosynthesis of silver nanoparticles using *Stenotrophomonas rhizophila* and its application as a disinfectant agent of water. *European Journal of Experimental Biology*. vol. 4, no. 1, pp. 662-669.

[10] Okolo, J. C. Nweke C. O., Nwabueze R. N., Dike C. U. and E.Nwanyanwu C. 2007. Toxicity of phenolic compounds to oxidoreductases of *Acinetobacter* species isolated from a tropical soil. *Scientific Research and Essay,* Vol. 2, no. 7, pp. 244-250.

[11] Conrado M., Cabiol P., Manual M., Rafael B.and Francisco P. 1999. Prokaryotic Nitrate Reduction: Molecular Properties and Functional Distinction among Bacterial Nitrate Reductases. *Journal of Bacteriology,* vol. 181, no. 21, pp. 6573–6584.

[12] Shubhasis D., Nirony D. and Tapan K. 2014. Application od Response Surface methodology (RSM) in statistical optimization and pharmaceutical characterization of matrix tablet formulation using mmMetforming HCL as a model drug. *International Journal of Sciences*, vol. 1, no. 2, pp. 1-6.

[13] Kenji A., Riu S.and Hiroshi N. 1981. Isolation and Identification of Respiratory Nitrate Reductase-Producing Bacteria from Soil and Production of the Enzyme. *Agriculture Biological Chemistry,* vol. 45, no. 4, pp. 817-822.

[14] Jon P. C., Ya hsin H., Stephen S. and David J. R. 1995. Soil and Sediment Bacteria Capable of Aerobic Nitrate Respiration. *Applied and environmental microbiology*, vol. 61, no. 8, pp. 2852-2858.

[15] Antonio L., Jesu D., Sabah E., Conrado M., Jose M.and Ferna N. 2002. Nitrate is reduced by heterotrophic bacteria but not transferred to *Prochlorococcus* in non-axenic cultures, *FEMS Microbiology Ecology,* vol. 41,pp. 151-160.

[16] Marangon J., Paes P. de Sousa, Moura I., Brondino C., Moura J. and González P. 2012. Substrate-dependent modulation of the enzymatic catalytic activity: Reduction of nitrate, chlorate and perchlorate by respiratory nitrate reductase from *Marinobacter hydrocarbonoclasticus* 617. *Biochimica et Biophysica Acta,* vol. 1817, pp. 1072–1082.

[17] Morozkina E. and Zvyagilskaya R. 2007. Nitrate Reductases: Structure, Functions, and Effect of Stress Factors. *Biochemistry (Moscow),* vol. 72, no. 10, pp. 1151-1160**.**

[18] Felgate H., Giannopoulos G., Sullivan M., Gates A., Clarke T., Baggs E., Rowley S. and Richardson D. 2012. The impact of copper, nitrate and carbon status on the emission of nitrous oxide by two species of bacteria with biochemically distinct denitrification pathways. *Environmental Microbiology,* vol. 14, no. 7, pp. 1788–1800.

[19] Takahashi J., Johchi N. and Fujita H. 1989. Inhibitory effects of sulphur compounds, copper and tungsten on nitrate reduction by mixed rumen micro-organisms. *British Journal of Nutrition,* vol. 61, pp. 741-748.

[20] Priyadarshini B., Mugeraya G. and Sandhyavali M. 2012. Effect of media conistitents on microbial enzyme activity. *International Journal of Pharmaceutical, Chemical and Biological Science,* vol. 2, no. 3, pp. 236-241.

[21] Sharma R. 2012b. Inhibition of Nitric Oxide Synthase Gene Expression: In Vivo Imaging Approaches of Nitric Oxide with Multimodal Imaging. In: Enzyme Inhibition: Concepts and Bioapplications. *Chapter 8, In Tech Web Publishers, Croatia*. ISBN, vol. 979.

[22] Francisco B., Pedro M., José A. and Luca D. 2010. Optimization of low-cost medium for very high gravity ethanol fermentations by *Saccharomyces cerevisiae* using statistical experimental designs. *Bioresource Technology,* vol. 101, pp. 7856–7863.

[23] Nordiyanah A., Ahmad F., Naziz S., Norkasmani A. and Rosna M. 2013. Optimization of Extraction Parameters by Using Response Surface Methodology, Purification, and Identification of Anthocyanin Pigments in *Melastoma malabathricum* Fruit. *The Scientific World Journal.*

[24] Yuan Y., Lu Z., Huang L., Bie X., Lu F. and Li Y.,2006. Optimization of a medium for enhancing nicotine biodegradation by *Ochrobactrum intermedium* DN2. *Journal of Applied Microbiology,* vol. 101, pp. 691–697.

[25] Nicholas D., Redmond W. and right M. 1964. Effects of Cultural Conditions on Nitrate Reductase in *Photobacterium sepia*. *Journal of genetic Microbiology,* vol. 35, pp. 401-410.

[26] Kim S., Song S. and Yoo Y. 2006. Characterization of membrane-bounnitrate reductase from denitrifying bacteria *Ochrobactrum anthropiSY509*. *Biotechnology and Bioprocess Engineering,* vol. 11, pp. 32-37.

[27] Mahmood Q., Hua B., Caia J., Zhenga P., Azimc M., Jilani G. and Islama E. 2009. Isolation of *Ochrobactrum sp*.QZ2 from sulfide and nitrite treatment system. *Journal of Hazardous Materials,* vol. 165, pp. 558–565.

[28] Cyplik P., Grajek W., Marecik R. and Kroliczak P. 2007. Effect of macro/micro nutrients and carbon source over the denitrification rate of *Haloferax denitrificans* archaeon. *Enzyme and Microbial Technology,* vol. 40, pp. 212–220.

[29] Liang S., Zhao M., Lu L., Wang C., Zhao L. and Liu W. 2011. Isolation and characteristic of an aerobic denitrifier with high nitrogen removal efficiency. *African Journal of Biotechnology,* vol. 10, no. 52, pp. 10648-10656.

[30] Vaidyanathan R., Kalishwaralal K., Gopalram S. and Gurunathan S. 2009. Nanosilver— The burgeoning therapeutic molecule and its green synthesis. *Biotechnology Advances,* vol. 27, pp. 924–937.

[31] El-Batal A., Amin M., Shehata M. and Hallol M. 2013. Synthesis of Silver Nanoparticles by *Bacillus stearothermophilus* Using Gamma Radiation and Their Antimicrobial Activity. *World Applied Sciences Journal,* vol. 22, no. 1, pp. 01-16.

[32 Al-Kadya] A., Gabera M., Hussein M. and Ebeida E. 2011. Structural and fluorescence quenching characterization of hematite nanoparticles. *Spectrochimica Acta Part A,* vol. 83, pp. 398– 405.

[33] Farahmandjou M. and Soflaee F. 2015. Synthesis and Characterization of α-Fe_2O_3 Nanoparticles by Simple Co-Precipitation Method. *Physics Chemical Research*. vol. 3, no. 3, pp. 193-198.

[34] Phuan Y., Chong M., Zhu T., Yong S., and Chan E. 2014. Effects of annealing temperature on the physicochemical, optical and photoelectrochemical properties of nanostructured hematite thin films prepared via electrodeposition method. *Materials Research Bulletin*.

[35] Batin M. and. Popescu V, 2011. Synthesis and characterization of iron oxide powders. *Powder Metallurgy Progress*. vol. 11, no. 4, pp. 202-205.

[36] Balamurughan M., Mohanraj S., Kodhaiyolii S. and Pugalenthi V. 2014. Ocimum sanctum leaf extract mediated green synthesis of iron oxide nanoparticles: spectroscopic and microscopic studies. *Journal of Chemical and Pharmaceutical Sciences.* pp. 201-204.

[37] Nidhin M., Indumathy R., Sreeram K. and Balachandran U. 2008. Synthesis of iron oxide nanoparticles of narrow size distribution on polysaccharide templates" *Bulltain Material Science.* vol. 31, no. 1, pp. 93–96.

[38] Joya, Bar _on-Jaimez J. and Barba-Ortega J. 2013. Preparation and characterization of Fe2O3 nanoparticles M. *Journal of Physics: Conference Series 466.*

[39] Park B., Song D., Kim H., Choi B., Lee H. and Lee J. 2009. The structural basis of lipopolysaccharide recognition by the TLR4–MD-2 complex. *Nature letters,* vol. 458, no. 30.

[40] Cohen G. N. 2011. The Outer Membrane of Gram-negative Bacteria and the Cytoplasmic Membrane. *Microbial Biochemistry.*

[41] Sugiyama N., Minami, Ishii Y., and Amano F. 2013. Inhibition of Lon protease by bacterial lipopolisaccharide (LPS) though N.inhibition of ATPase. *Advances in Bioscience and Biotechnology,* vol. 4, pp. 590-598.

[42] Ulyanov N. and James T. 2010. RNA structural motifs that entail hydrogen bonds involving sugar–phosphate backbone atoms of RNA. *New Journal of Chemistry* vol. 34, no. 5, pp. 910–917.

[43] Bong C., Malfatti F., Azam F., Obayasi Y. and Suzuki S*. 2010.* The Effect of Zinc Exposure on the Bacteria Abundance and Proteolytic Activity in Seawater. *Interdisciplinary Studies on Environmental Chemistry — Biological Responses to Contaminants, Eds., N. Hamamura, S. Suzuki, S. Mendo, C. M. Barroso, H. Iwata and S. Tanabe,* pp. 57–63.

[44] Lujun Z. 2009. Bioparticle Separation in Microfluidic Devices for in-Line Application. MSc. Thesis, *Royal Institute of Technology, Stockholm, Sweden*.

[45] Saeb A., Alshammari A., Al-Brahim H. and Al-Rubeaan K. 2014. Production of Silver Nanoparticles with Strong and Stable Antimicrobial Activity against Highly Pathogenic and Multidrug Resistant Bacteria. *Scientific World Journal.*

[46] Li C. 2004. Rheological properties of aqueous nanometric alumina suspensions" *PHD thesis, Iwoa State University*.

[47] Dukhovich F., Darkhovskii S., Gorbatova M. B.,. Kurochkin E. N. 2003. Molecular Recognition: Pharmacological Aspects. *New York: Nova Science Publishers*, p. 35.

[48] Matei E., Predescu A., Vasile E.and Predescu A. 2011. Properties of magnetic iron oxides used as materials for wastewater treatment. *Journal of Physics: Conference Series* 304.

[49] Filiz E. and Koç I. 2014 silico sequence analysis and homology modeling of predicted beta-amylase 7-like protein *in Brachypodium distachyon* L. *Journal of BioScience and Biotechnology.* vol. 3, no. 1, pp,61-67.

[50] Nilsson I. and Heijne G. 1990. Fine-Tuning the Topology of a Polytopic Membrane Protein: Role of Positively and Negatively Charged Amino Acids. *Cell.* vol. 62,pp. 1135-1141.

[51] Hua Y., Lua P., Zhanga Y., Lia L. and Chen S. 2010. Characterization of an aspartate-dependent acid survival system in *Yersinia pseudotuberculosis. FEDB Letters.* vol. 584, no.11, pp. 2311–2314.

[52] Guenot J., Fletterick R. J., and Kollman P. 1994. A negative electrostatic determinant mediates the association between the *Escherichia coli* frp repressor and its operator DNA. *Protein Science,* vol. 3, pp. 1276-1285.

[53] Zaki S., Eltarahony M., Elkady M., and Abd-El-Haleem D. 2014. The Use of Bioflocculant and Bioflocculant-Producing *Bacillus mojavensis* Strain 32A to Synthesize Silver Nanoparticles. *Journal of Nanomaterials.*

[54] Rajeshkumar S. Kannan C. and Annadura G. 2012. Green synthesis of silver nanoparticles using marine brown algea *Turbinaria conoides* and its antibacterial activity. *International Journal of Pharm and Bio Science.* vol. 3, no. 4, pp. 502 – 510.

[55] Madhavia V., Prasad T.and Madhavi G. 2013. Synthesis and spectral characterization of iron based micro and nanoparticles. *International Journal of Nanomaterials and Biostructures.* vol. 3, no. 2, pp. 31-34.

[56] Pal, S. 2014. Antimicrobial activity of iron oxide nanoparticles. *M.Sc., Thesis, Department of life science national institute of technology ROURKELA, Oressa. India.*

[57] Yadav V. and Fulekar H. 2014. Isolation and Charcterization of Iron Nanoparticles from Coal Fly Ash from Gandhinagar (Gujarat) Thermal Power Plant (A Mechanical Method of Isolation). *International Journal of Engineering Research & Technology.* vol. 3, no. 6.

[58] Deepak V., Kalishwaralal K., Pandian S., and Gurunathan S. 2011. An Insight into the Bacterial Biogenesis of Silver Nanoparticles, Industrial Production and Scale-up. *Metal Nanoparticles in Microbiology*.

[59] Varshney R., Bhadauria S.and Gaur M. 2012. A Review: Biological Synthesis Of Silver and Copper Nanoparticles. *Nano Biomedical Engneering,* vol. 4, no. 2, pp. 99-106.

[60] Elblbesy M., Madbouly K .A. and Hamdan T. 2014. Bio-synthesis of magnetite nanoparticles by bacteria. *American Journal of Nano Research and Application,* vol. 2, no. 5, pp. 98-103.